

The expected thermal precursors of gamma-ray bursts in the internal shock model

Frédéric Daigne^{1,2} and Robert Mochkovitch³

¹ *Max-Planck-Institut für Astrophysik, Karl-Schwarzschild-Str 1., 81748 Garching bei München, Germany*

² *Present address: CEA/DSM/DAPNIA, Service d’Astrophysique, C.E. Saclay, 91191 Gif sur Yvette Cedex, France*

³ *Institut d’Astrophysique de Paris, 98 bis bd. Arago 75014 Paris, France*

10 November 2018

ABSTRACT

The prompt emission of gamma-ray bursts probably comes from a highly relativistic wind which converts part of its kinetic energy into radiation via the formation of shocks within the wind itself. Such "internal shocks" can occur if the wind is generated with a highly non uniform distribution of the Lorentz factor. We estimate the expected photospheric emission of such a relativistic wind when it becomes transparent. We compare this thermal emission (temporal profile + spectrum) to the non-thermal emission produced by the internal shocks. In most cases, we predict a rather bright thermal emission that should already have been detected. This favors acceleration mechanisms for the wind where the initial energy input is under magnetic rather than thermal form. Such scenarios can produce thermal X-ray precursors comparable to those observed by GINGA and WATCH/GRANAT.

Key words: Gamma-rays: bursts – Radiation mechanisms: non-thermal – Radiation mechanisms: thermal – Hydrodynamics – Relativity

1 INTRODUCTION

The cosmological origin of long duration gamma-ray bursts (hereafter GRBs) has been firmly established since the discovery of their optical counterparts in 1997 (van Paradijs et al. 1997). These late and fading counterparts, the so called afterglows, have now been detected in many bursts, and in different spectral ranges: X-rays, optical and radio bands. The redshift has been measured for about 20 GRBs from $z = 0.43$ to $z = 4.5$. The corresponding isotropic equivalent energy radiated by these GRBs in the gamma-ray range goes from $5 \cdot 10^{51}$ erg to $2 \cdot 10^{54}$ erg. The beaming factor that has to be taken into account to obtain the real amount of radiated energy can be deduced from afterglow observations (achromatic break in the lightcurve, Rhoads (1999)). Current estimates lead to a total energy radiated in gamma-rays of about $0.5 - 1 \cdot 10^{51}$ erg (Frail et al. 2001). The most discussed scenario to explain the GRB phenomenon is made of three steps :

Central engine : The source of GRBs must be able to release a very large amount of energy in a few seconds. The two most popular candidates are either the merger of compact objects (neutron star binaries or neutron star–black hole systems (Narayan et al. 1992; Mochkovitch et al. 1993)) or the gravitational collapse of a massive star into a black hole (collapsars/hypernovae (Woosley 1993; Paczynski 1998)). Such events lead to the formation of

very similar systems made of a stellar mass black hole surrounded by a thick torus. The collapsar model seems to be favored in the case of long bursts by observational evidences that GRBs are located well inside their host galaxy and often associated to star-forming regions (Paczynski 1998; Djorgovski et al. 2001). The released energy is first injected into an optically thick wind, which is accelerated via an unknown mechanism, probably involving MHD processes (Thompson 1994; Meszaros & Rees 1997; Spruit et al. 2001) and becomes eventually relativistic. The existence of such a relativistic wind has been directly inferred from the observations of radio scintillation in GRB 970508 (Frail et al. 1997) and is also needed to solve the compactness problem and avoid photon-photon annihilation along the line of sight. Average Lorentz factors larger than 100 are required (Baring & Harding 1997; Lithwick & Sari 2001). The next two steps explain how the kinetic energy of this relativistic wind is converted into radiation at large distances from the source, when the wind has become optically thin.

Internal shocks : the production of gamma-rays is usually associated to the formation of shocks within the wind itself (Rees & Meszaros 1994). Such internal shocks can appear if the initial distribution of the Lorentz factor is highly variable, which is very likely considering the unsteady nature of the envisaged sources (MacFadyen & Woosley 1999). This

model has been studied in details (Kobayashi et al. 1997; Daigne & Mochkovitch 1998, 2000). The main difficulties which are encountered are a rather low efficiency for the conversion of the wind kinetic energy into gamma-rays (a few percents only) and problems in reproducing with synchrotron emission the slope of the low energy part of the spectrum (Ghisellini et al. 2000). Despite this difficulty, the model can successfully reproduce the main features of the bursts observed by BATSE.

External shock : the relativistic wind is decelerated later by the external medium. This phase of deceleration is probably the best understood of the three steps and reproduces very well the afterglow properties (Wijers et al. 1997). The dynamics of the wind during the deceleration phase is described by the solution of the relativistic Sedov problem (Blandford & McKee 1976) and the observed afterglow is due to synchrotron emission produced by relativistic electrons accelerated behind the strong forward shock propagating in the external medium (Sari et al. 1998).

The work presented in this paper focuses on the prompt emission. The spectrum of this emission as observed by BATSE and Beppo-SAX is non-thermal and is well fitted by the 4-parameter ‘‘GRB-function’’ proposed by Band et al. (1993). This function is made of two smoothly connected power-laws. This non-thermal emission probably originates from the radiation of a population of highly relativistic electrons accelerated behind the shock waves propagating within the wind during the internal shock phase.

Prior to the internal shock phase, the relativistic wind has to become transparent. At this transition, a thermal emission is produced, that could contribute to the observed prompt emission. Parts of the wind can also become opaque at larger radii if internal shocks create pairs in large number. These opaque regions can produce additional thermal components when they become transparent again (Mészáros & Rees 2000). Other thermal contributions can be expected, for example when the jet breaks out at the boundary of the stellar envelope in the collapsar scenario (Ramirez-Ruiz et al. 2002). In this paper, we restrict our analysis to the photospheric thermal component. A similar problem has been studied by Lyutikov & Usov (2000) in the different context of strongly magnetized winds emitted by rapidly rotating pulsars.

The paper is organized as follows : in sect. 2 we obtain the position of the photosphere of a relativistic wind with a highly variable initial distribution of the Lorentz factor, as expected in the internal shock model. We then compute the corresponding photospheric thermal emission in sect. 3 and compare it to the non-thermal emission from the internal shocks in sect. 4. The results are discussed in sect. 5 and the conclusions are summarized in sect. 6.

2 THE PHOTOSPHERE OF A RELATIVISTIC WIND

2.1 Photospheric radius

We do not discuss in this paper the nature of the source which is initially responsible for the energy release leading

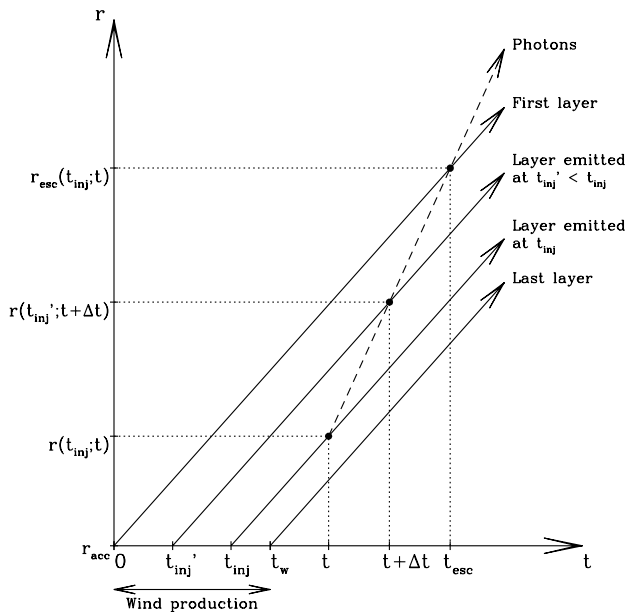


Figure 1. Sketch of the plane t - r : the solid line arrows show the paths of the layers produced by the source at radius r_{acc} from $t = 0$ to $t = t_w$. The dashed line arrow shows the path of the photons emitted at time t by the layer produced at time t_{inj} . These photons will cross the layer produced at time $t'_{inj} < t_{inj}$ after a duration Δt . They escape when they cross the first layer of the wind produced at $t = 0$.

to the gamma-ray burst. We suppose that a relativistic wind carrying the energy has emerged from the source, with an average Lorentz factor $\bar{\Gamma} \gtrsim 100$. We assume that the acceleration is complete at a distance r_{acc} from the source where the ultra-relativistic wind is characterized by an energy injection rate $\dot{E}(t_{inj})$ and an initial distribution of Lorentz factor $\Gamma(t_{inj})$. This corresponds to a mass flux $\dot{M}(t_{inj}) = \dot{E}(t_{inj})/\Gamma(t_{inj})c^2$, with \dot{E} and \dot{M} being the isotropic equivalent energy and mass injection rates. This wind production process lasts from $t_{inj} = 0$ to $t_{inj} = t_w$ (all these quantities are defined in the fixed frame of the source).

In this section we are interested in computing when the layer emitted by the source at t_{inj} will become transparent. We assume that the wind is still optically thick at r_{acc} , and that it becomes transparent before the internal shock phase and before it is decelerated by the external medium. We can then consider that each layer is evolving with a constant Lorentz factor so that at time t , the layer emitted at t_{inj} is located at

$$r(t_{inj}, t) \simeq r_{acc} + \left(1 - \frac{1}{2\Gamma^2(t_{inj})}\right) c(t - t_{inj}) . \quad (1)$$

Let us consider photons emitted at t by the layer ejected by the source at t_{inj} (see fig. 1). If they escape from the relativistic wind, these photons will have to cross all the layers emitted from $t'_{inj} = 0$ to $t'_{inj} = t_{inj}$. Precisely, they cross the layer ejected at t'_{inj} after

$$\Delta t \simeq 2\Gamma^2(t'_{inj}) \frac{\Delta r}{c} , \quad (2)$$

where Δr is the spatial separation at the emission time t

between the layer produced at t'_{inj} and the emitting layer produced at time t_{inj} . This distance is the initial separation $c(t_{\text{inj}} - t'_{\text{inj}})$ plus a correction growing with time due to the difference of Lorentz factor between the two layers :

$$\begin{aligned} \Delta r &= r(t'_{\text{inj}}, t) - r(t_{\text{inj}}, t) \\ &\simeq \left(1 - \frac{1}{2\Gamma^2(t'_{\text{inj}})}\right) c(t_{\text{inj}} - t'_{\text{inj}}) \\ &\quad + \frac{1}{2} \frac{\Gamma^2(t'_{\text{inj}}) - \Gamma^2(t_{\text{inj}})}{\Gamma^2(t'_{\text{inj}}) \Gamma^2(t_{\text{inj}})} c(t - t_{\text{inj}}) . \end{aligned} \quad (3)$$

The first term is very close to the initial separation and the second term is small as long as the process we consider takes place well before the internal shock phase. The photons escape from the wind when they cross the first layer emitted at $t'_{\text{inj}} = 0$ at time

$$t_{\text{esc}} \simeq t + 2\Gamma^2(0) \left(t_{\text{inj}} + \frac{1}{2} \frac{\Gamma^2(0) - \Gamma^2(t_{\text{inj}})}{\Gamma^2(0)\Gamma^2(t_{\text{inj}})} (t - t_{\text{inj}}) \right) \quad (4)$$

and at radius $r_{\text{esc}}(t_{\text{inj}}; t) = r(t_{\text{inj}}; t) + c(t_{\text{esc}} - t)$. The corresponding distance is $2\Gamma^2(0)$ times larger than the initial separation between the emitting layer and the front of the wind. The total optical depth for these photons is given by

$$\tau(t_{\text{inj}}, t) = \int_{r(t_{\text{inj}}, t)}^{r_{\text{esc}}(t_{\text{inj}}, t)} d\tau(r) . \quad (5)$$

The elementary contribution $d\tau(r)$ to the optical depth is a Lorentz invariant (Abramowicz et al. 1991) and is more easily estimated in the comoving frame of the layer crossed by the photons at r :

$$d\tau(r) = \kappa \rho' dl'(r) , \quad (6)$$

where κ and ρ' are the opacity and the comoving density of the layer. The length $dl'(r)$ is computed by a Lorentz transformation from the fixed frame to the comoving frame of the layer. We take into account the fact that when photons cover a distance dr , the corresponding duration is $dt = dr/c$ so that

$$dl'(r) = \Gamma(dr - vdt) \simeq \Gamma \left[1 - \left(1 - \frac{1}{2\Gamma^2}\right) \right] dr \simeq \frac{dr}{2\Gamma} . \quad (7)$$

The comoving density is given by

$$\rho' \simeq \frac{1}{\Gamma} \frac{\dot{M}}{4\pi r^2 c} . \quad (8)$$

Here all the physical quantities like Γ , \dot{M} , etc. have the value corresponding to the layer crossed by the photons at r , i.e. the layer emitted at t'_{inj} solution of (from eq. 2)

$$r = r(t_{\text{inj}}, t) + 2\Gamma^2(t'_{\text{inj}})\Delta r , \quad (9)$$

where Δr is given by eq. 3. The final expression for the total optical depth is

$$\tau(t_{\text{inj}}, t) \simeq \int_{r(t_{\text{inj}}, t)}^{r_{\text{esc}}(t_{\text{inj}}, t)} \frac{\kappa \dot{M}}{8\pi \Gamma^2 r^2 c} dr . \quad (10)$$

We define the photospheric radius $r_{\text{ph}}(t_{\text{inj}})$ of the layer emitted at t_{inj} by

$$r_{\text{ph}}(t_{\text{inj}}) = r(t_{\text{inj}}, t) \text{ with } \tau(t_{\text{inj}}, t) = 1 . \quad (11)$$

To estimate this radius, we still need to specify the opacity.

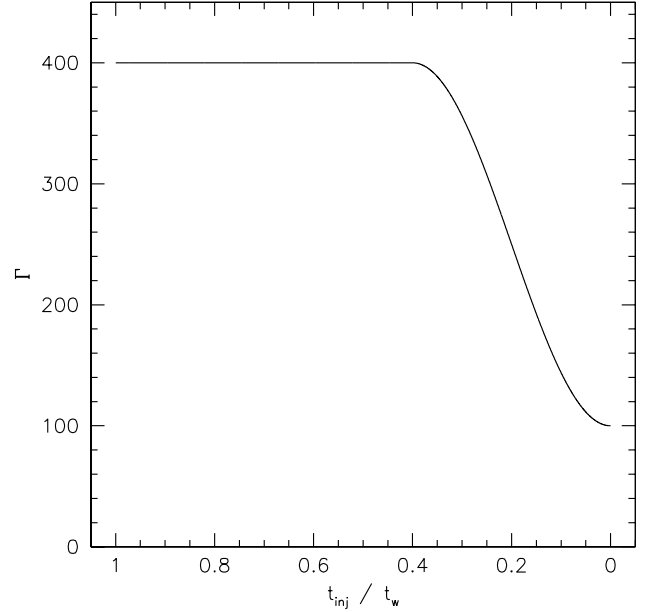


Figure 2. A single pulse burst : initial distribution of the Lorentz factor (example considered in sec. 2.4). The Lorentz factor Γ is plotted as a function of the injection time t_{inj} . As a constant energy injection rate \dot{E} is assumed, the masses of the fast ($\Gamma = 400$) and “slow” parts ($\Gamma = 100 \rightarrow 400$) are equal.

We consider here the phase when the acceleration is complete. The internal energy has already been almost entirely converted into kinetic energy. Pairs have annihilated and do not contribute to the opacity. Then the optical depth is due to the ambient electrons and the opacity is given by the Thomson opacity $\kappa = \kappa_{\text{T}}$. In the following, when a numerical value is needed, we use $\kappa = 0.2$ (i.e a number of electrons per nucleon $Y_e = 0.5$).

2.2 The case of a constant Lorentz factor

In the case of an homogeneous wind where \dot{E} , \dot{M} and Γ are constant, we have

$$\tau(t_{\text{inj}}, t) \simeq \frac{\kappa \dot{M} t_{\text{inj}}}{4\pi r(t_{\text{inj}}, t) r_{\text{esc}}(t_{\text{inj}}, t)} . \quad (12)$$

There are two limiting cases :

$$\tau(t_{\text{inj}}, t) \simeq \frac{\kappa \dot{M} t_{\text{inj}}}{4\pi r^2(t_{\text{inj}}, t)} \text{ if } r(t_{\text{inj}}, t) \gg 2\Gamma^2 ct_{\text{inj}} \quad (13)$$

or

$$\tau(t_{\text{inj}}, t) \simeq \frac{\kappa \dot{M}}{8\pi c \Gamma^2 r(t_{\text{inj}}, t)} \text{ if } r(t_{\text{inj}}, t) \ll 2\Gamma^2 ct_{\text{inj}} . \quad (14)$$

The corresponding photospheric radius of the layer ejected at t_{inj} is given by

$$r_{\text{ph}}(t_{\text{inj}}) \simeq \left(\frac{\kappa \dot{M} t_{\text{inj}}}{4\pi} \right)^{1/2} \text{ if } \frac{\dot{E}}{\Gamma^5 t_{\text{inj}}} \gg \frac{16\pi c^4}{\kappa} \quad (15)$$

or

$$r_{\text{ph}}(t_{\text{inj}}) \simeq \frac{\kappa \dot{M}}{8\pi c \Gamma^2} \text{ if } \frac{\dot{E}}{\Gamma^5 t_{\text{inj}}} \ll \frac{16\pi c^4}{\kappa} , \quad (16)$$

where we have replaced \dot{M} by $\dot{E}/\Gamma c^2$. The condition $\dot{E}/\Gamma^5 t_{\text{inj}} \ll 16\pi c^4/\kappa$ reads

$$\frac{\dot{E}_{52}}{\Gamma_2^5 t_{\text{inj}}} \ll \frac{200}{\kappa_{0.2}}, \quad (17)$$

which is usually true. Here \dot{E}_{52} , Γ_2 and $\kappa_{0.2}$ are respectively \dot{E} , Γ and κ in unit of 10^{52} erg/s, 10^2 and 0.2. Then, the photospheric radius is the same for all the layers and is given by (eq. 16) :

$$r_{\text{ph}} = 3.0 \cdot 10^{12} \kappa_{0.2} \dot{E}_{52} \Gamma_2^{-3} \text{ cm} . \quad (18)$$

If we estimate r_{acc} by the saturation radius Γr_0 which is predicted in the fireball model, we get

$$r_{\text{acc}} \simeq 9 \cdot 10^8 \mu_1 \Gamma_2 \text{ cm} \quad (19)$$

for a typical initial radius r_0 taken to be the last stable orbit at three Schwarzschild radii around a non rotating black hole of mass $M_{\text{BH}} = 10\mu_1 M_{\odot}$. It is clear that r_{ph} is much larger than r_{acc} as expected.

2.3 The case of a variable Lorentz factor

We now consider the case where the initial distribution of the Lorentz factor is variable. We use the simple model that has been developed by Daigne & Mochkovitch (1998). The wind is made of a collection of ‘‘solid’’ layers ejected regularly on a time scale Δt_{inj} with a Lorentz factor, a mass and an energy Γ_i , $M_i = \dot{M}_i \Delta t_{\text{inj}}$ and $E_i = \dot{E}_i \Delta t_{\text{inj}}$ where $i = 1$ corresponds to the first layer produced at $t_{\text{inj}} = 0$. Photons emitted by the layer i_0 when it is located at r_{i_0} travel through a total optical depth

$$\tau(r_{i_0}) = \frac{\kappa}{8\pi c^3} \sum_{i \leq i_0} \frac{\dot{E}_i}{\Gamma_i^3} \left(\frac{1}{r_i^{\text{in}}} - \frac{1}{r_i^{\text{out}}} \right), \quad (20)$$

where r_i^{in} and r_i^{out} are the radii at which the photons enter and escape the layer i . We have (from eq. 9)

$$r_i^{\text{in}} \simeq 2\Gamma_i^2 \left[c(i_0 - i) \Delta t_{\text{inj}} + \frac{r_{i_0}}{2\Gamma_{i_0}^2} \right] \quad (21)$$

and

$$r_i^{\text{out}} \simeq r_i^{\text{in}} + 2\Gamma_i^2 c \Delta t_{\text{inj}} . \quad (22)$$

In the following, we use the exact formula (20) to compute the optical depth and we solve numerically $\tau(r_{\text{ph}}) = 1$ to get the photospheric radius of the layer i_0 . An approximate value is obtained under the assumption that the opacity is dominated by the contribution of the layer i_0 where photons are emitted. We then have :

$$r_{\text{ph}}^{\text{approx}} \simeq \frac{\kappa \dot{E}_{i_0}}{8\pi c^3 \Gamma_{i_0}^3}, \quad (23)$$

for $r_{\text{ph}} \ll 2\Gamma_{i_0}^2 c t_{\text{inj}}$ (with $t_{\text{inj}} = (i_0 - 1)\Delta t_{\text{inj}}$). This is usually true except for the first layers ($t_{\text{inj}} \rightarrow 0$).

2.4 Example : a single pulse burst

We consider the case of a relativistic wind ejected during $t_w = 10$ s with a constant energy injection rate $\dot{E} = 10^{52}$ erg/s and an initial distribution of Lorentz factor represented in fig. 2. Such a simple initial distribution has already

been considered in Daigne & Mochkovitch (1998, 2000) and leads to a typical single pulse burst. We use $\Delta t_{\text{inj}} = 2 \cdot 10^{-3}$ s so that the wind is made of 5000 layers. For each layer i we compute the photospheric radius $r_{\text{ph } i}$ and the radius $r_{\text{esc } i}$ where the photons emitted at the photosphere escape from the relativistic wind. The result is plotted in fig 3 as a function of the mass coordinate M_i . Notice that except for the front of the wind, the approximate value of r_{ph} given by eq. 23 works extremely well. An interesting result is that the deepest layers in the wind become transparent before the layers located at the front. This is due to the fact that photons emitted by these layers cross the front at larger radii when the density has already strongly decreased (one can see that r_{esc} for these layers is larger than at the front). The photospheric radius goes from $\simeq 4.7 \cdot 10^{10}$ cm to $\simeq 3.0 \cdot 10^{12}$ cm. We can check now that this is well before the internal shocks form or the deceleration of the wind by the external medium becomes efficient. The typical radius of the internal shocks is given by

$$r_{\text{IS}} \simeq f \bar{\Gamma}^2 c t_{\text{var}}, \quad (24)$$

where t_{var} is the characteristic time scale for the variations of the Lorentz factor and f is a numerical factor depending on the details of the initial distribution of the Lorentz factor (f will be smaller for high contrasts of Γ). For a typical average Lorentz factor $\bar{\Gamma} \gtrsim 100$ we have

$$r_{\text{IS}} \simeq 3 \cdot 10^{14} f \bar{\Gamma}^2 t_{\text{var}} \text{ cm} \quad (25)$$

and we immediately see that except for very small values of f or very short time scales t_{var} , the typical radius of the internal shocks is larger than the photospheric radius. The deceleration of the wind by the external medium occurs even further away, except in very dense wind environments.

3 TIME PROFILE AND SPECTRUM OF THE PHOTOSPHERIC EMISSION

3.1 Photospheric luminosity

In the framework of the fireball model, the temperature and luminosity of a layer at its photospheric radius r_{ph} are given (in the fixed frame) by (see e.g. Piran (1999))

$$kT_{\text{ph}} \simeq kT^0 \left(\frac{r_{\text{ph}}}{r_{\text{acc}}} \right)^{-2/3} \quad (26)$$

and

$$L_{\text{ph}} \simeq \dot{E} \left(\frac{r_{\text{ph}}}{r_{\text{acc}}} \right)^{-2/3} \quad (27)$$

(in this section we omit the index i . Everything applies to each layer). The radius r_{acc} is the saturation radius defined by eq. 19 and the initial blackbody temperature of the layer is (Mészáros & Rees 2000)

$$kT^0 \simeq 1.3 \dot{E}_{52}^{1/4} \mu_1^{-1/2} \text{ MeV}. \quad (28)$$

Deviations from the predictions of the standard fireball model are however possible. The central engine of gamma-ray bursts is still poorly understood and the acceleration mechanism not clearly identified. A large fraction of the energy released by the source may be for instance initially stored under magnetic form (Spruit et al. 2001). In this case, the wind is not as hot as in the standard fireball

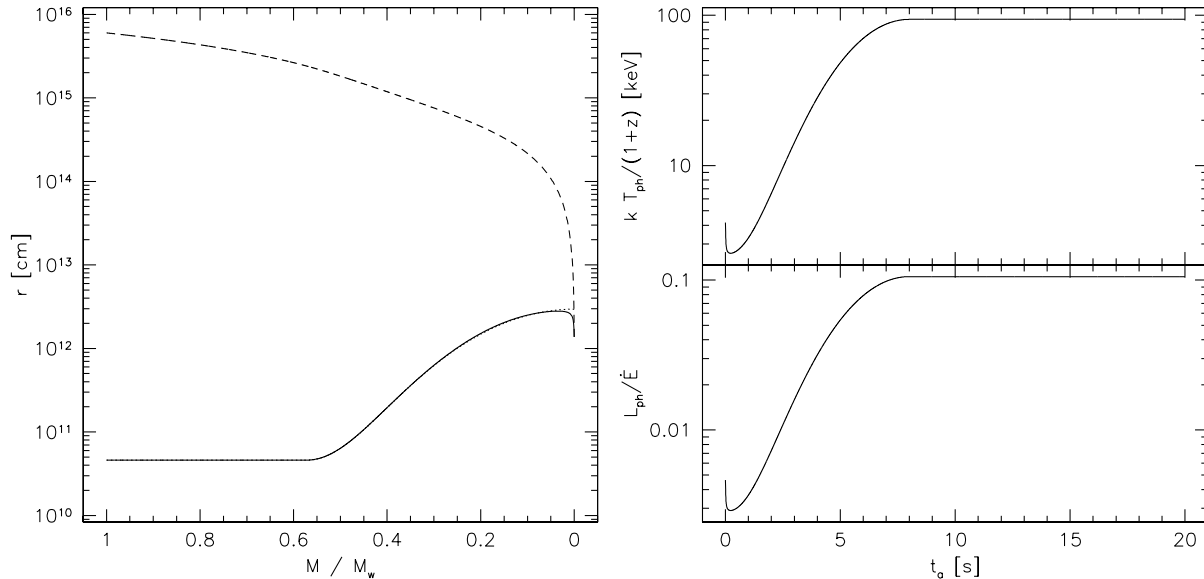


Figure 3. A single pulse burst : photosphere of the relativistic wind (example considered in secs. 2.4 and 3.3). **Left** : the photospheric radius r_{ph} is plotted as a function of the mass coordinate of layers within the relativistic wind (solid line). The approximate value eq. 23 (dotted line) is also shown : the only noticeable difference is at the front of the wind ($M \rightarrow 0$). The dashed line shows the radius at which the photons emitted at the photospheric radius of each layer escape from the wind. **Right** : the photospheric luminosity L_{ph} and observed temperature $kT_{\text{ph}} / (1+z)$ are plotted as a function of the arrival time t_a for $\lambda = 1$. A redshift $z = 1$ is assumed.

model and the photospheric luminosity is also smaller. An extreme case would be the magnetic acceleration of a cold wind where the photospheric temperature and luminosity are negligible.

Whatever the physics of this early phase may be, it should necessarily have the two following properties in common with the standard fireball model :

(i) *The acceleration mechanism must have a good efficiency.* The observed isotropic equivalent gamma-ray luminosity L_γ is indeed very high. To account for it, the internal shock model requires a isotropic equivalent kinetic energy flux

$$\dot{E}_{52} = \frac{L_\gamma 51}{f_{\gamma 0.1}}, \quad (29)$$

where $L_\gamma 51$ is the observed isotropic equivalent gamma-ray luminosity in unit of 10^{51} erg/s and $f_{\gamma 0.1}$ is the efficiency for the conversion of kinetic energy into gamma-rays in unit of 0.1. As this kinetic energy flux is already very high, we cannot expect the source to release much more energy. Therefore the need for an efficient acceleration is unavoidable. This means that beyond r_{acc} , the energy flux is completely dominated by the kinetic energy flux, like beyond the saturation radius in the standard fireball model. The main difference may probably be the value of r_{acc} compared to the standard saturation radius $\sim \Gamma r_0$.

(ii) *Beyond r_{acc} the wind experiences a phase of adiabatic cooling due to spherical expansion.* An efficient acceleration indeed implies that the wind is still optically thick at r_{acc} . In this case kT_{ph} and L_{ph} decrease as $r^{-2/3}$ beyond r_{acc} like in the standard fireball model. Only the initial value of the temperature and the internal energy density at the end

of the acceleration phase can be different from those of the standard fireball model.

To account for our poor knowledge of the physical process responsible for the acceleration of the wind, we define λ as the fraction of the energy which is initially injected under internal energy form. In the standard fireball model $\lambda = 1$ whereas $0 \leq \lambda \leq 1$ in the other possible cases. With this definition we have

$$kT_{\text{ph}} \simeq \lambda^{1/4} kT^0 \left(\frac{r_{\text{ph}}}{r_{\text{acc}}} \right)^{-2/3} \quad (30)$$

and

$$L_{\text{ph}} \simeq \lambda \dot{E} \left(\frac{r_{\text{ph}}}{r_{\text{acc}}} \right)^{-2/3}. \quad (31)$$

The acceleration radius r_{acc} may differ from the saturation radius given by eq. 19. However, we will show below that the relevant quantity to estimate the photospheric emission is the ratio $L_{\text{ph}} / kT_{\text{ph}}$ which does not depend on r_{acc} , as long as the photospheric radius is large compared to r_{acc} .

3.2 Spectrum, count rate and arrival time of the photospheric emission

We suppose that the photosphere radiates as a blackbody at temperature kT_{ph} . This is clearly a simplifying assumption as scattering processes may play an important role when the opacity is $\tau \gtrsim 1$. However, we believe that the possible deviations from a pure blackbody will not change our main conclusions. We also neglect corrections in the spectrum due to angular effects affecting photons originating from different regions of the emitting shell. We then consider that the emitted photons have a Planck distribution which is in the source frame :

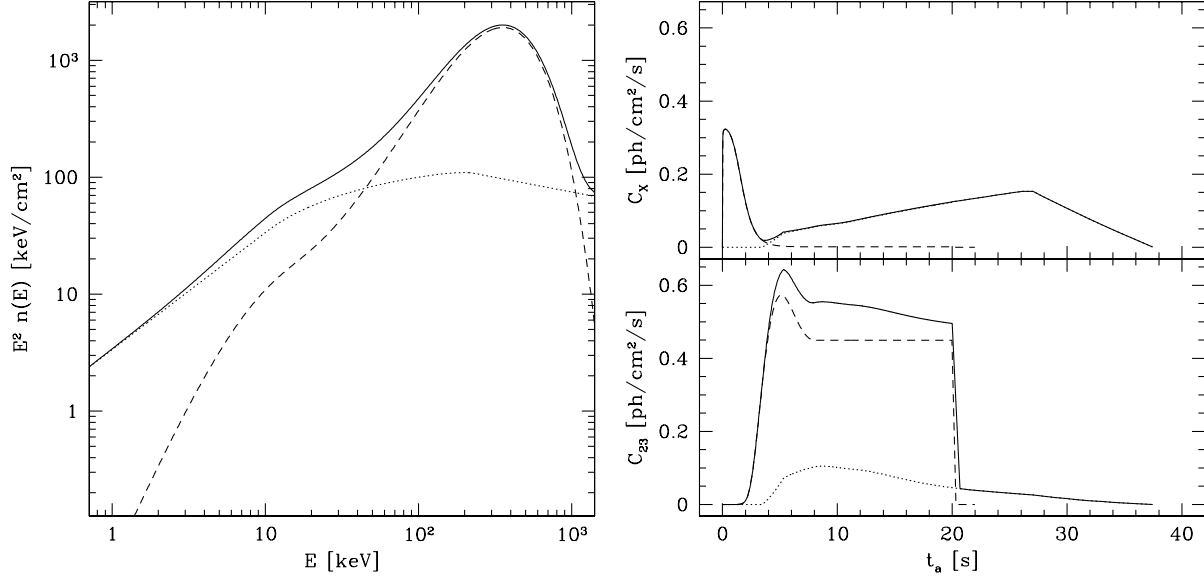


Figure 4. A single pulse burst : spectrum and time profile (example considered in secs. 2.4 and 3.3). A redshift $z = 1$ is assumed. **Left :** the spectrum $E^2 n(E)$ is plotted as a function of the photon energy in keV. **Right :** the count rate is plotted as a function of arrival time in the 3.5–8.5 keV band (top) and in the 50–300 keV band (bottom). The dashed line corresponds to the photospheric emission, the dotted line to the non-thermal emission from the internal shocks and the solid line to the total emission. The global spectrum is dominated by the luminous contribution from the photosphere of the rapid part of the wind, peaking at about $3.92 kT_{\text{ph}} \simeq 370$ keV.

$$\frac{dn^{\text{ph}}(E)}{dEdt} = \frac{1}{\mathcal{I}_{\text{Planck}}} \frac{L_{\text{ph}}}{(kT_{\text{ph}})^4} \frac{E^2}{\exp\left(\frac{E}{kT_{\text{ph}}}\right) - 1}, \quad (32)$$

where $\mathcal{I}_{\text{Planck}} = \int_0^{+\infty} \frac{x^3}{\exp x - 1} dx = \frac{\pi^4}{15}$. Taking into account the redshift z of the source, the observer will detect a photon flux at energy E (observer frame) which is given by

$$C^{\text{ph}}(E) = \frac{1}{\mathcal{I}_{\text{Planck}}} \frac{L_{\text{ph}}}{4\pi D_L^2} \left(\frac{1+z}{kT_{\text{ph}}}\right)^4 \frac{E^2}{\exp\left(\frac{(1+z)E}{kT_{\text{ph}}}\right) - 1}, \quad (33)$$

where D_L is the luminosity distance at redshift z . The corresponding count rate in the energy band $[E_1; E_2]$ is

$$C_{12}^{\text{ph}} = \frac{L_{\text{ph}}}{4\pi D_L^2} \frac{1+z}{kT_{\text{ph}}} \frac{\mathcal{I}_{12}^{\text{ph}}}{\mathcal{I}_{\text{Planck}}}, \quad (34)$$

where $\mathcal{I}_{12}^{\text{ph}} = \int_{x_1}^{x_2} \frac{x^2}{\exp x - 1} dx$ and $x_{1,2} = (1+z)E_{1,2}/kT_{\text{ph}}$. It is interesting to notice that the ratio $L_{\text{ph}}/kT_{\text{ph}}$ depends neither on the shell radius nor on the saturation radius :

$$\frac{L_{\text{ph}}}{kT_{\text{ph}}} \simeq 5.0 \cdot 10^{57} \lambda^{3/4} \dot{E}_{52}^{3/4} \mu_1^{1/2} \text{ ph/s}. \quad (35)$$

Then the count rate in the energy band $[E_1; E_2]$ is given by

$$C_{12}^{\text{ph}} \simeq 4.0 \frac{1+z}{D_{28}^2} \lambda^{3/4} \dot{E}_{52}^{3/4} \mu_1^{1/2} \frac{\mathcal{I}_{12}^{\text{ph}}}{\mathcal{I}_{\text{Planck}}} \text{ ph/cm}^2/\text{s}, \quad (36)$$

where D_{28} is the luminosity distance D_L in unit of 10^{28} cm. The emitted photons will be detected at the arrival time t_a (relatively to a signal travelling at the speed of light) :

$$t_a = t_{\text{ph}} - \frac{r_{\text{ph}}}{c}, \quad (37)$$

where t_{ph} is the time when the layer reaches the radius r_{ph} . We get

$$t_a \simeq t_{\text{inj}} + \frac{r_{\text{ph}}}{2\Gamma^2 c}. \quad (38)$$

With the approximate value of r_{ph} given by eq. 23, we have

$$t_a^{\text{approx}} \simeq t_{\text{inj}} + \frac{\kappa \dot{E}}{8\pi c^4 \Gamma^5}. \quad (39)$$

We already checked in the previous section that the second term is negligible compared to t_{inj} . Then $t_a \simeq t_{\text{inj}}$. The spreading of arrival times over a duration $\Delta t_a \simeq r_{\text{ph}}/2c\Gamma^2$ due to the curvature of the emitting surface is also negligible for the same reason (of course these estimations of t_a have to be multiplied by $1+z$ in the observer frame to account for the redshift). The fact that $t_a \simeq (1+z)t_{\text{inj}}$ shows that the time profile of the photospheric emission, if observed, would provide a detailed direct information about the initial distribution of Lorentz factor in the wind.

3.3 Example : a single pulse burst

We consider the same distribution of the Lorentz factor and injected power as in sec. 2.4 and we now compute the thermal emission of the photosphere for a standard fireball ($\lambda = 1$). Fig. 3 shows the luminosity and the temperature at the photosphere as a function of the arrival time of photons. We did not use the approximations given by Eqs. 26–27 which are strictly valid only for $r_{\text{ph}} \gg r_{\text{acc}}$ but we used the exact solution of the fireball equations (see e.g. Piran (1999)). We adopted a redshift $z = 1$. Fig. 4 shows the corresponding integrated spectrum of the photospheric emission and the time profile in two energy bands : 3.5–8.5 keV which is one of the X-ray bands of *Beppo-SAX* and 50–300 keV which is the 2+3 gamma-ray band of *BATSE*. The photospheric emission of the “slow” part ($t_{\text{inj}} = 0 \rightarrow 4$ s and $t_a \simeq (1+z)t_{\text{inj}} = 0 \rightarrow 8$ s) has a temperature kT_{ph} increas-

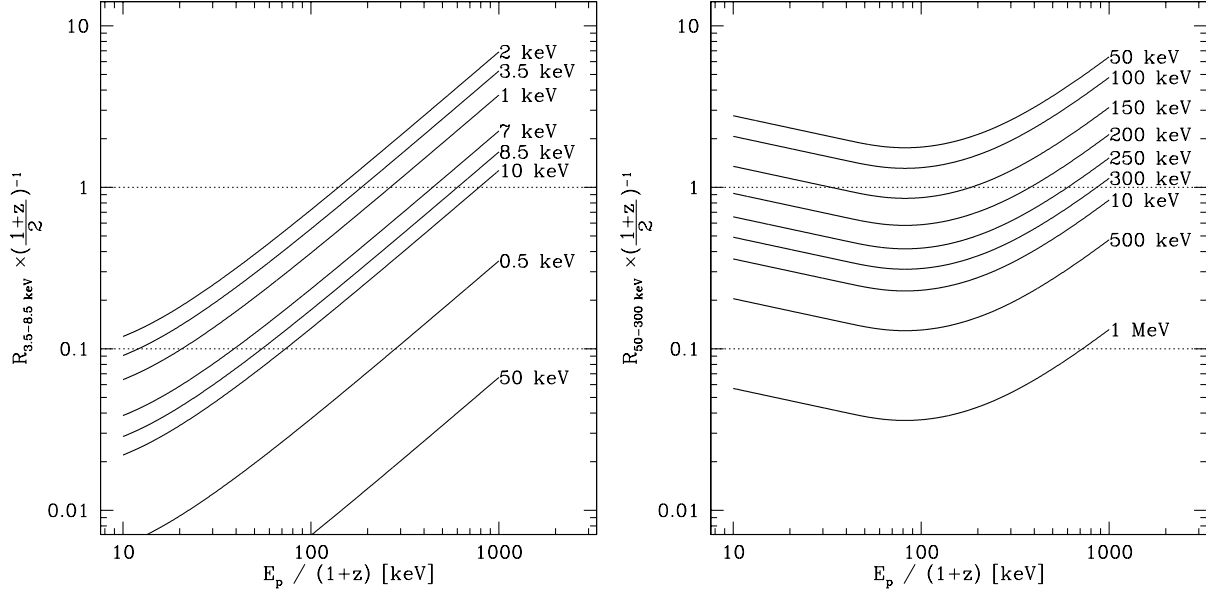


Figure 5. The ratio of the count rate due to the photospheric emission over the count rate due to the internal shocks is plotted as a function of the peak energy of the non-thermal spectrum (observer frame) for different values of the photospheric temperature $kT_{\text{ph}}/(1+z)$ in the observer frame. The spectrum of the non-thermal emission from the internal shocks is computed using the GRB-function with $\alpha = -1.0$ and $\beta = -2.25$. The following parameters have been adopted: $\lambda = 1$, $\dot{E}_{52} = 1$, $f_\gamma = 0.1$, $\mu_1 = 1$. *Left*: X-ray band 3.5–8.5 keV; *Right*: gamma-ray band 50–300 keV.

ing from 4.2 to 94 keV. It initially produces a pulse only visible in the X-ray band ($t_a \simeq 0 \rightarrow 3$ s). Then, the count rate rises in the gamma-ray band, reaches a maximum at ~ 5 s when $kT_{\text{ph}} \simeq 48$ keV and starts to decrease (although the temperature is still increasing) because the peak energy ($\sim 3.92 kT_{\text{ph}}$) becomes larger than 300 keV. The rapid part ($t_{\text{inj}} = 4 \rightarrow 10$ s and $t_a \simeq (1+z)t_{\text{inj}} = 8 \rightarrow 20$ s) has a constant temperature of 94 keV, so that the count rate is constant and mainly visible in the gamma-ray range.

4 COMPARISON WITH THE EMISSION FROM THE INTERNAL SHOCKS

4.1 Time profile and spectrum of the emission from the internal shocks

We now estimate the count rate due to the emission of the internal shocks. Their luminosity can be written as $L_{\text{IS}} \simeq f_\gamma \dot{E}$, with $f_\gamma \simeq f_d \alpha_e$. The efficiency f_d of the dissipation process is the fraction of kinetic energy which is converted into internal energy behind the shocks; α_e is the fraction of the internal energy which is injected into relativistic electrons, which then radiate to produce the gamma-ray burst, with a radiative efficiency f_{rad} which is assumed to be very close to 1. We do not discuss here the details of the radiative processes and we simply assume that the emitted photons have a spectral distribution given by the ‘‘GRB-function’’ (Band et al. 1993):

$$\frac{dn^{\text{IS}}(E)}{dE dt} = \frac{1}{\mathcal{I}_{\text{Band}}} \frac{L_{\text{IS}}}{E_p^2} \mathcal{B}\left(\frac{E}{E_p}\right). \quad (40)$$

The peak energy E_p is defined as the maximum of $E^2 dn^{\text{IS}}(E)/dE/dt$ and is measured here in the source frame, so that the peak energy in the observer frame is $E_p/(1+z)$.

The function $\mathcal{B}(x)$ has two parameters, the low and high energy slopes α and β and is given by

$$\mathcal{B}(x) = \begin{cases} x^\alpha \exp(-(2+\alpha)x) & \text{if } x \leq \frac{\alpha-\beta}{2+\alpha} \\ x^\beta \left(\frac{\alpha-\beta}{2+\alpha}\right)^{\alpha-\beta} \exp(\beta-\alpha) & \text{otherwise} \end{cases} \quad (41)$$

The integral $\mathcal{I}_{\text{Band}} = \int_0^{+\infty} x \mathcal{B}(x) dx$ depends only on α and β which we assume to be constant during the whole burst. The observed photon flux at energy E is given by

$$C^{\text{IS}}(E) = \frac{1}{\mathcal{I}_{\text{Band}}} \frac{L_{\text{IS}}}{4\pi D_L^2} \left(\frac{1+z}{E_p}\right)^2 \mathcal{B}\left(\frac{(1+z)E}{E_p}\right) \quad (42)$$

and the corresponding count rate in the energy band $[E_1; E_2]$ is

$$C_{12}^{\text{IS}} = 2.5 \frac{1+z}{D_{28}^2} f_{\gamma 0.1} \dot{E}_{52} \left(\frac{E_p}{200 \text{ keV}}\right)^{-1} \frac{\mathcal{I}_{12}^{\text{IS}}}{\mathcal{I}_{\text{Band}}} \text{ph/cm}^2/\text{s}, \quad (43)$$

where $\mathcal{I}_{12}^{\text{IS}} = \int_{x_1}^{x_2} \mathcal{B}(x) dx$ with $x_{1,2} = (1+z)E_{1,2}/E_p$.

4.2 Comparison with the photospheric emission

We now define R_{12} as the ratio of the count rate due to the photospheric emission over the count rate due to the internal shocks:

$$R_{12} = 1.6 \lambda^{3/4} f_{\gamma 0.1}^{-1} \dot{E}_{52}^{-1/4} \mu_1^{1/2} \frac{E_p}{200 \text{ keV}} \frac{\mathcal{I}_{\text{Band}} \mathcal{I}_{12}^{\text{ph}}}{\mathcal{I}_{\text{Planck}} \mathcal{I}_{12}^{\text{IS}}}. \quad (44)$$

Fig. 5 shows the value of R_{12} for two energy bands (X- and gamma-rays) as a function of E_p assuming different values of the photospheric temperature kT_{ph} . We have adopted $\alpha = -1.0$ and $\beta = -2.25$ which are the typical slopes observed in GRBs (Preece et al. 2000). It is clear that the photospheric emission will show up in a given band ($R_{12} \gtrsim 0.1$) when the observed temperature $kT_{\text{ph}}/(1+z)$ of the photosphere

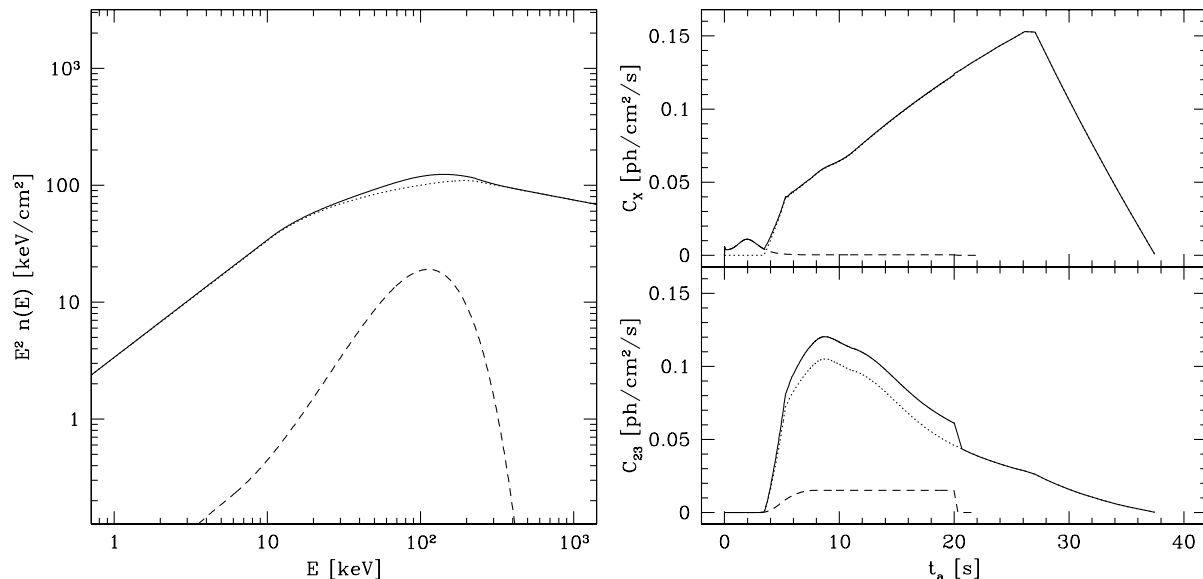


Figure 6. A single pulse burst with a less luminous photosphere : spectrum and time profile (example considered in sec. 4.3). The wind is the same as in sec. 2.4 but we now assume $\lambda = 0.01$. The redshift is $z = 1$. **Left :** the spectrum $E^2 n(E)$ is plotted as a function of the photon energy in keV. **Right :** the count rate is plotted as a function of arrival time in the 3.5–8.5 keV band (top) and in the 50–300 keV band (bottom). As in fig. 4, the dashed line is the contribution of the photospheric emission, the dotted line is the contribution of the internal shocks and the solid line is the total count rate (photosphere + internal shocks).

crosses this band. These results show that with the prediction of the standard fireball model for the photospheric temperature and luminosity, it is very difficult to prevent the photospheric emission from being easily detectable¹ either in the X-ray or gamma-ray range. The presence of a bright thermal component is not supported by the observations : the gamma-ray burst prompt emission, as seen by *BATSE*, is clearly non-thermal. Concerning the X-ray emission, especially at the beginning of the burst, more observations with better spectroscopic capabilities than *Beppo-SAX* will be necessary to check whether a thermal component is present or not.

4.3 Example : a single pulse burst

We have computed the emission of the internal shocks in the single pulse burst considered in secs. 2.4 and 3.3 using the simple model developed by Daigne & Mochkovitch (1998). The result is shown in fig. 4. The equipartition parameters have been chosen so that the peak energy of the emission from the internal shocks is 200 keV. As the photosphere reaches a temperature $kT_{\text{ph}}/(1+z)$ as high as 94 keV, the study made in the previous subsection predicts that the photospheric emission should be easily detectable, which is clearly visible in fig. 4.

To recover a burst which is dominated by the non-thermal emission of the internal shocks in the gamma-ray

range, eq. 44 indicates that either f_γ must increase or λ must decrease. The first solution is then to have more efficient internal shocks. In the example presented in fig. 4, the efficiency is low : $f_\gamma \simeq 0.02$. As there are many uncertainties in the radiative processes leading to the observed gamma-ray emission, one could hope that f_γ is indeed very close to f_d , the fraction of kinetic energy dissipated in internal shocks. However, the efficiency f_d will never exceed a few 10^{-1} . Therefore, even in the ideal case where $f_\gamma \sim f_d$, one cannot expect to have f_γ larger than 0.3–0.4. We have checked that this is not enough to avoid a easily detectable photospheric emission.

The only remaining solution is then to assume that the photosphere is less hot and luminous than what is predicted in the standard fireball model, i.e. to decrease the value of λ in eqs. 30–31. To have a spectrum entirely dominated by the non-thermal component we have to adopt $\lambda \lesssim 0.01$, which means that less than 1 percent of the energy initially released by the source is injected under internal energy form into a “standard” fireball. Such a situation is shown in fig. 6 where we have computed the photospheric emission of the single pulse burst with $\lambda = 0.01$. It is impossible to detect the thermal emission of the photosphere neither in the gamma-ray profile nor in the global spectrum. However, in the X-ray range, one can notice that during 2 seconds before the internal shock emission starts, there is a thermal precursor whose intensity is about 8 percents of the intensity at maximum in the main pulse.

We have finally considered the effect of pair creation during the internal shock phase. The optical depth for pair creation is given by (Mészáros & Rees 2000) :

¹ Notice that E_p is defined as the peak energy of the non-thermal emission of the internal shocks and is of course no more the peak energy of the total observed spectrum when the photospheric emission is dominant.

$$\tau_{\pm} \simeq \frac{\alpha_{\pm} L_{\text{IS}} \sigma_{\text{T}}}{4\pi r (m_e c^2) \Gamma^3 c}, \quad (45)$$

where α_{\pm} is the fraction of the energy radiated in photons above the pair creation threshold. Our internal shock model allows the computation of τ_{\pm} at each shock radius. For the example considered here, τ_{\pm} never exceeds $6 \cdot 10^{-2}$. For larger \dot{E} and / or smaller Lorentz factors (in this case, if \dot{E} is increased by a factor of ~ 20 or if all Lorentz factors are divided by ~ 2), τ_{\pm} increases and pair creation can become important, especially for shocks occurring at small radii. We do not compute in this paper the detailed internal shock spectrum for this case where an additional thermal component can be expected.

5 DISCUSSION

5.1 X-ray thermal precursors

In the GRBs observed by BeppoSAX the X-ray and gamma-ray emission usually start simultaneously or the gamma-ray emission starts earlier. Usually, no evidence is found for a thermal component in the spectrum (Frontera et al. 2000). Then, the prompt X-ray emission is probably due to the internal shocks like in the gamma-ray range. This implies that the photospheric emission must be present in these bursts only at a very low level, i.e. $\lambda \ll 1$ as explained in the previous section. However, in at least one case – GRB 990712 – evidence was found in the spectrum for the presence during the burst of a weak thermal component of temperature 1.3 keV (Frontera et al. 2001). In complement, a X-ray precursor activity has been detected in a few GRBs by GINGA (Murakami et al. 1991) and WATCH/GRANAT (Sazonov et al. 1998). In the observations carried out with the GRB detector onboard the GINGA satellite, X-ray precursors were detected between 1.5 and 10 keV in about one third of the GRBs. The spectrum of these X-ray precursors could be approximated by a black-body with temperatures between 1 and 2 keV. The WATCH catalog also includes several GRBs with X-ray precursors detected between 8 and 20 keV. As can be seen in the time profiles of these bursts (Sazonov et al. 1998), the X-ray precursor usually has a duration which is about 20-50% of the duration of the whole burst and its count rate in the 8-20 keV band reaches about 10-40% of the maximum count rate in the same band during the GRB.

As the study of the GINGA data shows evidence for a thermal origin, one can wonder whether these X-ray precursors are associated to the photospheric emission. This could be possible if the two following conditions are satisfied :

–*Condition (1)* The ratio of the photospheric over internal shock count rate as defined by eq. 44 must be small in the gamma-ray range but greater than a few 10% in the X-ray range. The region of the $kT_{\text{ph}} / (1+z) - \lambda / f_{\gamma}$ plane where such a condition can be achieved (using the energy bands of the WATCH experiment) is shown in fig. 7. We find that (i) the photospheric temperature $kT_{\text{ph}} / (1+z)$ must lie in the X-ray band, which is easily obtained if $\lambda \simeq 0.1$. (ii) the ratio λ / f_{γ} must be above a minimal value which is typically about 0.1 and decreases when the peak energy E_p increases.

–*Condition (2)* As no activity (thermal or non thermal) is detected in the gamma-ray band during the X-ray precursor,

the internal shock emission must start at the end of the precursor. We have shown in sec. 3.2 that the arrival time of the photons emitted by the layer ejected by the source at t_{inj} when it becomes transparent can be approximated by $t_{\text{a}} \simeq t_{\text{inj}}$. The arrival time of photons emitted by the internal shocks due to the collisions between two layers emitted at t'_{inj} and $t_{\text{inj}} > t'_{\text{inj}}$ (with $\Gamma(t_{\text{inj}}) > \Gamma(t'_{\text{inj}})$) is

$$t_{\text{a}} \simeq t_{\text{inj}} + \frac{t_{\text{inj}} - t'_{\text{inj}}}{\left(\Gamma(t_{\text{inj}})/\Gamma(t'_{\text{inj}})\right)^2 - 1}. \quad (46)$$

The only possibility to increase the delay between the beginning of the photospheric emission and the beginning of the internal shock emission is then to impose that the variability of the initial distribution of the Lorentz factor in the relativistic wind is initially low ($\Gamma(t_{\text{inj}})/\Gamma(t'_{\text{inj}}) \rightarrow 1$) and increases during the wind production by the source.

Condition (1) is easily achieved if the initial fraction of the energy released by the source under internal energy form is low. For instance, in fig. 6, one clearly sees a X-ray precursor lasting for about 10% of the total duration with an intensity of about 8% of the intensity at maximum (in the X-ray band). On the other hand, some of the precursors observed by GINGA and WATCH/GRANAT have longer durations. This is where condition (2), which is probably a stronger constraint, is important.

We propose the following interpretation for the presence or absence of a precursor : it is necessary to have $\lambda \ll 1$ in order to suppress a too strong thermal gamma-ray emission from the photosphere. This naturally leads to a prompt thermal X-ray activity, which then could be very frequent in GRBs. However this activity is too weak to be easily detected when it occurs simultaneously to the bright non-thermal emission from the internal shocks. It is only when it appears as a precursor activity that it can be clearly identified. This can happen if by chance the relativistic wind is initially produced with a smooth distribution so that the internal shock activity is delayed. The expected features of such precursors are very close to the properties of the X-ray precursors observed by GINGA and WATCH/GRANAT.

To check the validity of this interpretation one clearly needs more precise detections of the X-ray prompt emission of GRBs and especially a better characterization of the spectral properties of the X-ray precursors. If a black-body spectrum can be identified without any ambiguity, the corresponding temperature will be measured, which would constrain the λ parameter.

5.2 The optical photospheric emission

To recover a dominant non-thermal gamma-ray emission we need λ to be of a few percents or less. The corresponding Planck spectrum then peaks in the X-ray band : for instance, the burst considered in sec. 4.3 has a photospheric temperature in the range $kT_{\text{ph}} \simeq 2$ –100 keV for $\lambda = 1$ and $kT_{\text{ph}} \simeq 0.6$ –30 keV for $\lambda = 0.01$. It is interesting to estimate what is the photospheric emission for even lower values of λ and if it could be dominant in the optical and produce a prompt optical flash comparable to that observed

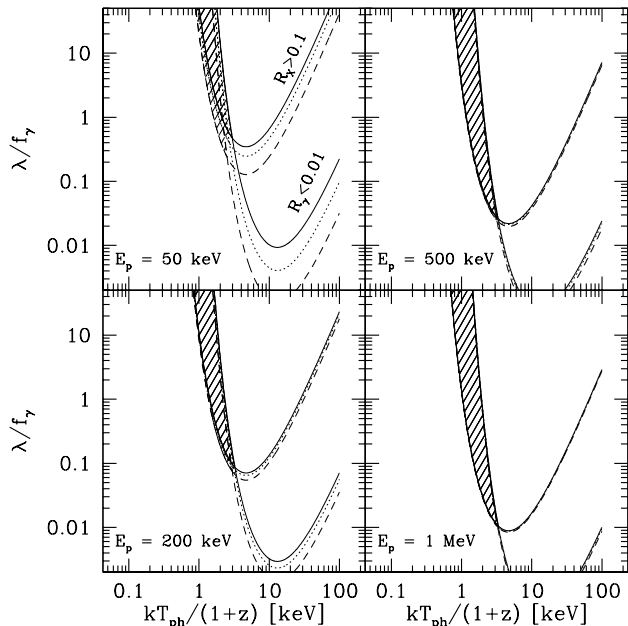


Figure 7. In the $kT_{\text{ph}}/(1+z)-\lambda/f_{\gamma}$ plane, the stripped area shows the region where the photospheric thermal emission is negligible in the 20-60 keV gamma-ray band of WATCH/GRANAT (count rate ratio smaller than 1%) but can be detected in the 8-20 keV X-ray band of the same experiment (count rate ratio greater than 10%). Each panel corresponds to a particular value of the peak energy E_p of the internal shock emission (respectively 50, 200, 500 and 1000 keV). The solid, dotted and dashed curves respectively correspond to $z = 0$, $z = 1$ and $z = 3$. The other parameters are $L_{\text{IS}} = f_{\gamma} \dot{E} = 10^{51}$ erg/s, $\alpha = -1$, and $\beta = -2.25$.

in GRB 990123 (Akerlof et al. 1999).

It is very unlikely that the photospheric emission peaks in the V band, because the photospheric temperature scales as $\lambda^{1/4}$. To decrease kT_{ph} from 100 keV to 1 eV, a very unrealistic value of $\lambda = (10^{-5})^4 = 10^{-20}$ is required! The V band then always lies in the Rayleigh-Jeans part of the photospheric spectrum where $\frac{dn^{\text{ph}}}{dE dt} \propto E$. GRB 990123 has an averaged spectrum which is well reproduced by the Band function with the following parameters: $\alpha = -0.6$, $\beta = -3.11$, $E_p = 720$ keV and photon flux $1.93 \cdot 10^{-3}$ ph/s/cm²/keV at 1 MeV (Briggs et al. 1999). The redshift of the source is $z = 1.6$. The corresponding internal shock luminosity is $L_{\text{IS}} = f_{\gamma} \dot{E} \simeq 8.6 \cdot 10^{52}$ erg/s. If we now assume that the internal shocks have no other contribution in the optical range than that given by the Band spectrum, their flux in the V band ($0.55 \mu\text{m}$) is $F_V^{\text{IS}} \simeq 4.9 \cdot 10^{-2}$ mJy, which is much too low to explain the optical flash reaching magnitude $m_V \sim 9$ (i.e. $F_V \simeq 0.92$ Jy) observed by ROTSE. In the Rayleigh-Jeans regime, the corresponding flux due to the thermal photospheric emission is even lower :

$$F_V^{\text{ph}} \simeq 2.3 \cdot 10^{-5} \left(\frac{\lambda}{f_{\gamma}} \right)^{3/4} \mu_1^{1/2} \left(\frac{kT_{\text{ph}}}{1 \text{ keV}} \right)^{-2} \text{ mJy} . \quad (47)$$

We then find that the photospheric optical emission is much too weak to explain the ROTSE observations. This result is mainly due to the fact that the photospheric luminosity decreases much faster with λ than the temperature.

6 CONCLUSIONS

In the framework of the internal shock model for gamma-ray bursts, we have computed in a detailed way the photospheric emission of an ultra-relativistic wind with a variable initial distribution of the Lorentz factor. We have compared the obtained spectrum and time profile to the non-thermal contribution of the internal shocks. Our main results are the following :

(1) *The photosphere in the standard fireball model is too hot and luminous.* In the standard fireball model where the initial temperature of the fireball is about 1 MeV, the internal energy is still large when the wind becomes transparent and the photosphere is therefore hot and luminous. The consequence is that the photospheric thermal component in the X-ray/gamma-ray range is in most cases at least as bright as the non-thermal component due to the internal shocks (even if the internal shock efficiency is high). This is in contradiction with the observations of BATSE and Beppo-SAX showing non-thermal spectra.

(2) *MHD winds are favored.* Results in much better agreement with the observations are obtained when it is assumed that only a small fraction λ of the energy released by the source is initially injected under internal energy form in a fireball. Most of the energy could for instance be initially under magnetic form, a large fraction of the Poynting flux being eventually converted into kinetic energy at large distances. For a typical internal shock efficiency of a few percents, values of $\lambda \lesssim 0.01$ are required, which means that not more than 1% of the energy is initially deposited in the ejected matter (whose initial temperature is then of about a few hundreds keV).

(3) *X-ray thermal precursors can be obtained.* A consequence of this strong assumption is that moderately low λ ($\lambda \simeq$ a few percents) lead to the presence of thermal X-ray precursors if the distribution of the Lorentz factor is not too variable in the initial phase of wind production. The characteristics of these precursors (spectral range, duration, intensity) are very comparable to the X-ray precursor activity observed in several GRBs by GINGA and WATCH/GRANAT.

(4) *The optical photospheric emission is very weak.* For very small λ values, the photospheric emission can be shifted to even lower energies. However, we have shown that it also becomes much too weak to explain the prompt optical emission observed by ROTSE in GRB 990123.

A good test of the results presented in this paper would be the detection of X-ray precursors by an instrument with good spectral capabilities, so that a thermal origin could be firmly established. A determination of the photospheric temperature would put an interesting constraint on the λ/f_{γ} ratio and then on the wind acceleration mechanism. Moreover, if the photospheric thermal emission could be clearly detected (for instance in the soft X-ray range), it would provide a direct information about the initial distribution of the Lorentz factor in the wind before the internal shocks start.

ACKNOWLEDGMENTS

F.D. acknowledges financial support from a postdoctoral fellowship from the French Spatial Agency (CNES).

REFERENCES

- Abramowicz M. A., Novikov I. D., Paczynski B., 1991, *ApJ*, 369, 175
- Akerlof C., Balsano R., Barthelemy S., Bloch J., Butterworth P., Casperson D., Cline T., Fletcher S., Frontera F., Gisler G., Heise J., Hills J., Kehoe R., Lee B., Marshall S., McKay T., Miller R., Piro L., Priedhorsky W., Szymanski J., Wren J., 1999, *Nature*, 398, 400
- Band D., Matteson J., Ford L., Schaefer B., Palmer D., Teegarden B., Cline T., Briggs M., Paciesas W., Pendleton G., Fishman G., Kouveliotou C., Meegan C., Wilson R., Lestrade P., 1993, *ApJ*, 413, 281
- Baring M. G., Harding A. K., 1997, *ApJ*, 491, 663
- Blandford R. D., McKee C. F., 1976, *Physics of Fluids*, 19, 1130
- Blandford R. D., Znajek R. L., 1977, *MNRAS*, 179, 433
- Briggs M. S., Band D. L., Kippen R. M., Preece R. D., Kouveliotou C., van Paradijs J., Share G. H., Murphy R. J., Matz S. M., Connors A., Winkler C., McConnell M. L., Ryan J. M., Williams O. R., Young C. A., Dingus B., Catelli J. R., Wijers R. A. M. J., 1999, *ApJ*, 524, 82
- Chevalier R. A., Li Z., 2000, *ApJ*, 536, 195
- Daigne F., Mochkovitch R., 1998, *MNRAS*, 296, 275
- Daigne F., Mochkovitch R., 2000, *A&A*, 358, 1157
- Djorgovski S. G., Kulkarni S. R., Bloom J. S., Frail D. A., Harrison F. A., Galama T. J., Reichart D., Castro S. M., Fox D., Sari R., Berger E., Price P., Yost S., Goodrich R., Chaffee F., 2001, in *Gamma-ray Bursts in the Afterglow Era The GRB Host Galaxies and Redshifts*. p. 218
- Frail D. A., Kulkarni S. R., Nicastro S. R., Feroci M., Taylor G. B., 1997, *Nature*, 389, 261
- Frail D. A., Kulkarni S. R., Sari R., Djorgovski S. G., Bloom J. S., Galama T. J., Reichart D. E., Berger E., Harrison F. A., Price P. A., Yost S. A., Diercks A., Goodrich R. W., Chaffee F., 2001, *ApJ*, 562, L55
- Frontera F., Amati L., Costa E., Muller J. M., Pian E., Piro L., Soffitta P., Tavani M., Castro-Tirado A., Dal Fiume D., Feroci M., Heise J., Masetti N., Nicastro L., Orlandini M., Palazzi E., Sari R., 2000, *ApJS*, 127, 59
- Frontera F., Amati L., Vietri M., Zand J. J. M. i., Costa E., Feroci M., Heise J., Masetti N., Nicastro L., Orlandini M., Palazzi E., Pian E., Piro L., Soffitta P., 2001, *ApJ*, 550, L47
- Ghisellini G., Celotti A., Lazzati D., 2000, *MNRAS*, 313, L1
- Kobayashi S., Piran T., Sari R., 1997, *ApJ*, 490, 92
- Lithwick Y., Sari R., 2001, *ApJ*, 555, 540
- Lytikov M., Usov V. V., 2000, *ApJ*, 543, L129
- Mészáros P., Rees M. J., 2000, *ApJ*, 530, 292
- MacFadyen A. I., Woosley S. E., 1999, *ApJ*, 524, 262
- Meszáros P., Rees M. J., 1997, *ApJ*, 482, L29
- Mochkovitch R., Hernanz M., Isern J., Martin X., 1993, *Nature*, 361, 236
- Murakami T., Inoue H., Nishimura J., van Paradijs J., Fenimore E. E., 1991, *Nature*, 350, 592
- Narayan R., Paczynski B., Piran T., 1992, *ApJ*, 395, L83
- Paczynski B., 1998, *ApJ*, 494, L45
- Panaitescu A., Kumar P., 2001, *ApJ*, 554, 667
- Piran T., 1999, *Physics Reports*, 314, 575
- Preece R. D., Briggs M. S., Mallozzi R. S., Pendleton G. N., Paciesas W. S., Band D. L., 2000, *ApJS*, 126, 19
- Ramirez-Ruiz E., MacFadyen A. I., Lazzati D., 2002, *MNRAS*, 331, 197
- Rees M. J., Meszaros P., 1994, *ApJ*, 430, L93
- Rhoads J. E., 1999, *ApJ*, 525, 737
- Sari R., Piran T., Narayan R., 1998, *ApJ*, 497, L17
- Sazonov S. Y., Sunyaev R. A., Terekhov O. V., Lund N., Brandt S., Castro-Tirado A. J., 1998, *A&ASS*, 129, 1
- Spruit H. C., Daigne F., Drenkhahn G., 2001, *A&A*, 369, 694
- Thompson C., 1994, *MNRAS*, 270, 480
- van Paradijs J., Groot P. J., Galama T., Kouveliotou C., Strom R. G., Telting J., Rutten R. G. M., Fishman G. J., Meegan C. A., Pettini M., Tanvir N., Bloom J., Pedersen H., Nordgaard-Nielsen H. U., Linden-Vornle M., Melnick J., van der Steene G., Bremer M., Naber R., Heise J., in 't Zand J., Costa E., Feroci M., Piro L., Frontera F., Zavattini G., Nicastro L., Palazzi E., Bennet K., Hanlon L., Parmar A., 1997, *Nature*, 386, 686
- Wijers R. A. M. J., Rees M. J., Meszaros P., 1997, *MNRAS*, 288, L51
- Woosley S. E., 1993, *ApJ*, 405, 273